Growth and morphology of tin nanoparticles obtained by the condensation of metal vapors

M. Francisco Melendrez[a] and C. Vargas-Hernández[b,c]
[a]*Department of Materials Engineering (DIMAT), Faculty of Engineering, University of Concepcion, 270 Edmundo, Larenas, Casilla 160-C, Concepción, Chile 4070409.*
[b]*Laboratorio de Propiedades Ópticas de Materiales GTA-POM, Universidad Nacional de Colombia, A.A 127, Manizales, Colombia.*
[c]*International Center for Nanotechnology and Advanced Materials, Department of Physics & Astronomy, University of Texas at San Antonio, Texas 78249-0631. USA.*

Recibido el 23 de julio de 2012; aceptado el 16 de octubre de 2012

Tin nanoparticles (Sn-Nps) were synthesized using the metal vapor condensation technique (MVC) in a metallic atoms reactor. The parameters used for synthesis in this study were the following: distance to the metal evaporation center (MEC), metal evaporated moles (MEM), and frosting and defrosting temperatures of substrates. The Sn-Np depositions were carried out with Sn bulk over glass substrates positioned vertically at different angles and distances to the MEC. The Sn-Np characterization was performed by TEM, SEM, selected area electron diffraction (SAED), and UV-Vis. The TEM micrographs evidenced particle sizes of 75 and 25 nm for depositions conducted at 3 and 10 cm above the MEC, respectively. The particle sizes depended significantly on the MEC, the substrate, and the MEM. The SAED revealed phases corresponding to SnO (tetragonal) and α-Sn in different crystalline orientations. The technique showed good reproducibility in terms of particle size, and it is an important source of nanostructured materials free of impurities, which are widely used for printing electronic circuits.

Keywords: Nanoparticles; thin film; metallic atoms.

Nanoparticulas de estaño fueron sintetizadas por la técnica de condensación de vapores metálicos (MVC) en un reactor de átomos metálicos. Los parámetros de síntesis fueron: distancia de los substratos respecto al centro de evaporación del metal (MEC), cantidad de moles evaporados del metal (MEM), tiempo de congelación y descongelación de los substratos antes de la evaporación del metal. El depósito de las nanoparticulas se realizó partiendo de Sn metálico, sobre substratos de vidrio colocados en posición vertical y en diferentes ángulos respecto al MEC. La caracterización se realizó por TEM, SEM, difracción de electrones de área seleccionada (SAED) y UV-Vis. Micrografias de TEM mostraron tamaños de partícula comprendidos entre 75 y 25 nm para distancias respecto al MEC de 3 y 10 cm, respectivamente. El tamaño de partícula dependió del MEC, el susbtrato y el MEM. La técnica SEAD reveló las fases correspondientes a SnO (tetragonal) y α-Sn en diferentes orientaciones cristalinas. La técnica empleada presento buena reproducibilidad en cuanto al tamaño de partícula y es una importante fuente de materiales nanoestructurados libres de impurezas, los cuales son muy utilizados para la impresión de circuitos electrónicos.

Descriptores: Nanopartículas; películas delgadas; átomos metálicos

PACS: 68.55.ag; 68.65.-k; 81.16.-c

1. Introduction

The synthesis of nanostructured materials has attracted considerable interest in several fields of chemistry, physics, and materials science due to their novel physical-chemical properties, which are significantly different from the corresponding properties of the same materials in the macroscopic phase [1-3]. Nanostructured materials exhibit many properties, such as grain size, large surface areas, homogeneity and highly reactive surfaces, that have attracted attention because of the various resulting applications and theoretical studies [4,5]. The properties of nanostructured materials are determined not only by the cluster size but also by the manner in which they are organized. The way that nanoclusters form nanostructures depends not only on the separation and the properties of inter-cluster interaction but also on the preparation method used [6].

To obtain metallic nanoparticles and some oxides, many techniques have been used, such as sol-gel [7], pulsed laser deposition [8], mechanochemical [9], wet-chemical synthesis [10,11], chemical liquid deposition (CLD) [12-15], electrochemical [16], thermal decomposition [17], microwave irradiation [18], metal vapor deposition [19], and sonochemical techniques [20]. For MVC synthesis, two types of reactions are used: (a) co-deposition with the metal to form a stabilized colloid by the solvation of clusters with organic molecules in a frozen matrix at 77 K via a technique known as CLD [21], and (b) direct deposition of metallic vapors over frozen substrates. In the latter case, nucleation is determined by the substrate temperature and by the metal evaporation speed. In some cases, the substrates are not frozen, and in others, the vapor deposition occurs with the substrates positioned horizontally either above or below the MEC.

Motivated to employ the varying properties of nanoparticles, such as non-linear optics, luminescence, electronics, optoelectronics, and others [22-25], on a technological level in several fields of science, we aimed to synthesize tin metal-

lic nanoparticles by MVC over thin glass substrates at the freezing point of liquid nitrogen. Unlike conventional techniques, our depositions were carried out on vertically positioned substrates placed at different angles and distances to the MEC in order to obtain homogeneous samples that were free of impurities. The Sn-Nps were obtained by controlling parameters such as MEC, MEM, and the freezing time of the glass substrates.

2. Materials and methods

The Sn-Nps were obtained in a tubular reactor for metallic atoms with frozen walls at the temperature of liquid nitrogen (77 K), which is also used for CLD synthesis. The main difference is the solvent; MVC does not use a co-deposition of metallic and organic vapors because only the metal is deposited on the substrate. In these reactions, a pressure of 1.013 Pa and a voltage of 35 amperes were used for 1 h, increasing the electric current at a rate of 0.1 A/min. Substrates were washed with aqua regia, distilled water and 2-propanol and dried at 50°C under vacuum for 5 h. Metallic tin powder was used (purchased from Aldrich), which was degasified by the standard freeze-thaw procedure using liquid nitrogen and further sonication for 30 minutes. The tubular reactor was washed with KOH/2-propanol and aqua regia to eliminate metal impurities and high vacuum silicon.

Glass substrates were placed inside the reactor at 3, 6, and 10 cm both above (+) and below (-) the MEC. In all reactions, the glass substrate was always positioned vertically with the same angle and distance to the MEC. See Fig. 1.

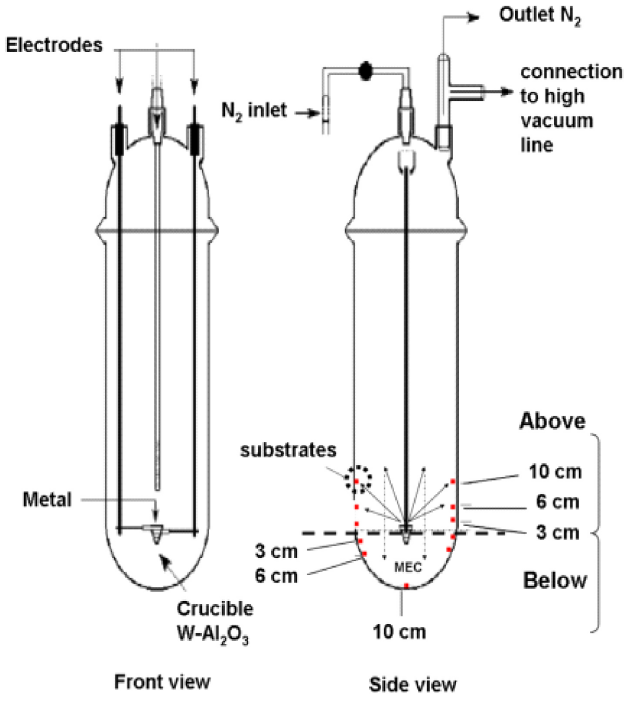

FIGURE 1. Tubular reactor for metallic atoms showing the positions and distances of thin glass substrates with respect to the MEC.

Prior to evaporation, the reactor was cooled to 77 K for 10, 60, and 120 minutes in order to study the effect of substrate temperature on particle size distribution. In each reaction, 8.4×10^{-05}(MEM1), 2.1×10^{-04} (MEM2) and 4.2×10^{-04}(MEM3) moles of Sn^0 were evaporated. After Sn-Np deposition, the system was isolated for 1, 30, 60, 90, and 120 minutes to study the effect of latency time on particle size. Latency is the time delay after evaporation and freezing beginning under inert atmosphere. During the latency time, the reactor is under high vacuum, without liquid nitrogen and with a Dewar flask to facilitate a slow defrosting. After finalizing the latency time, the defrosting operation of the reactor was finished with an extra-pure nitrogen flow for 30 minutes at room temperature. Substrates were removed from the reactor in inert atmosphere and were placed in a dry chamber to avoid Sn-Np oxidation.

Particle sizes were determined by histogram analysis, performed with the Jeol-JEM 1200 EXII Transmission electron microscope with a resolution of 4 Å. Thin glass substrates were reduced to 0.1 μm thicknesses and placed directly under the microscope observation. Particle size measurements were randomly taken and the data obtained were represented in a histogram, which provided information about particle size distribution. Additionally, normal distribution curve adjustments revealed the average size; Gaussian curves were also adjusted. Electron diffraction was carried out at 120 kV, 60 cm, K: 4.2 Å. The instrument calibration was performed with an Au film (Aldrich Chemical, 99.99 %). To obtain the UV-Vis spectra of nanoparticles, a UV-2450 (FIT B1-050) Shimadzu spectrophotometer was used. A glass substrate of standard thickness was used as a reference.

3. Results and discussion

The particle size distribution of the deposits was obtained by analysis of TEM micrographs. Table I summarizes the particle sizes according to MEC. TEM micrographs showed that the particle size varied significantly with the distance to MEC. Large particle sizes were obtained for depositions close to the metal evaporation center: 75 and 83 nm for substrates placed at (-) and (+) 3 cm to the MEC, respectively.

TABLE I. Particle size of the deposits over thin glass substrates. (+) Substrates above the MEC. (-) Substrates below the MEC, for MEM2

MEC (cm)	Substrate position (-)Below, (+)Above	Average particle size (nm)
10	(-)	25
6	(-)	33
3	(-)	75
3	(+)	83
6	(+)	61
10	(+)	41

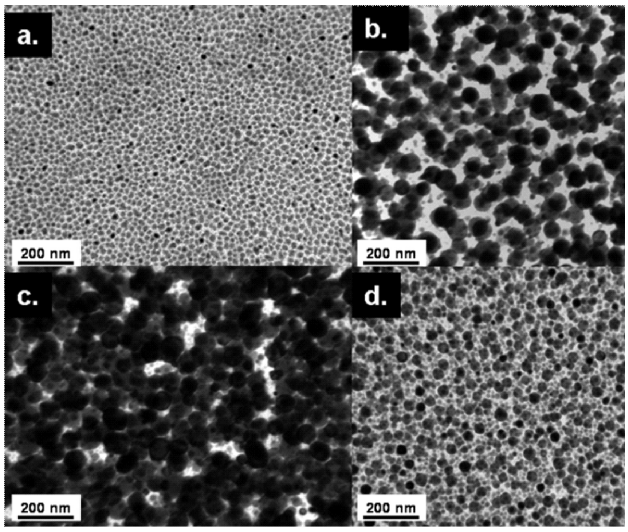

FIGURE 2. TEM micrographs of Sn-Nps: (a) (-) 3 cm, (b) (-10) cm, (c) (+) 3 cm, (d) (+) 10 cm. (+) Substrates above the MEC; (-) substrates below the MEC.

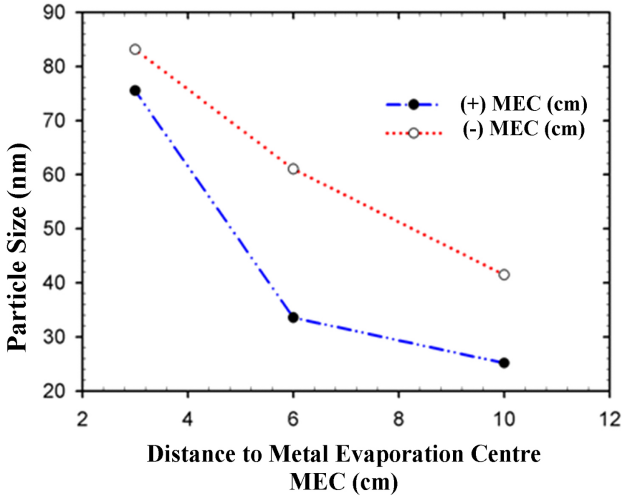

FIGURE 3. Behavior of particle size with respect to the distance to the MEC.

These values decrease as the substrate becomes more distant from the MEC, with particle sizes of 41 and 25 nm at (-) and (+) 10 cm to the MEC, respectively. For MEM2, smaller particle sizes were obtained for depositions below the MEC, whereas greater particle sizes were obtained for depositions above the MEC. These results differed from those reported by Cardenas *et al*., who obtained smaller bi-metallic and metallic tin particles by chemical liquid deposition [26]. Although MVC generates a greater particle size, this technique does not produce metal-solvent adducts, as does CLD. These adducts could modify the electronic properties of a metal, making them ineligible for usage in electronic devices.

In contrast, greater particle size and wide size distributions of Sn-Nps (50-300 nm) have been obtained by high-intensity ultrasound irradiation [27], as well as by solution dispersion techniques, which have produced Sn-Np sizes of 30-40 nm [28].

The main advantage of the MVC technique with respect to wet methods, as mentioned above, is the absence of impurities and co-reactants in the reaction system. This is the case of chemical reduction methods, chemical liquid deposition, chemical vapor deposition, and precursor thermal decomposition. Some of these techniques produce particles with a wide size distribution, uneven shapes and in many cases, fractal aggregates formed. Figure 2 (a-d) shows TEM micrographs for (-) 10, (-) 3, (+) 3, and (+) 10 cm to the MEC, for MEM2. For all deposits, regularly shaped spherical particles were an indicator of the efficiency of MVC for the production of metallic Nps.

In other metal evaporation techniques, such as ionized cluster beam (IBC) [29] and physical vacuum deposition (PVD) with charged cluster model (CCM), smaller and uniform size metallic particles (2-10 nm) have been obtained [30] over glass, Si and metal foil substrates. By MVC, it was possible to obtain particle sizes on the order of 10 nm, only decreasing the MEM (Fig. 8). It was also shown that the Sn-Nps agglomerated for substrates close to the MEC. The agglomeration is mainly due to (1) the large number of atoms in the gaseous state that increases the number of non-elastic collisions and (2) the short displacement of atoms in the MEC at the substrate. These characteristics produce the increase in the particle population and particle size in zones close to the MEC. Figure 3 illustrates the trends in particle size varying with distance to the MEC.

The atoms evaporate in all directions and angles, including the vertical direction, with high kinetic energy. In the gaseous state, atoms collide with one another, losing part of their initial kinetic energy and forming deposits on the substrates close to the MEC. The atoms and particles formed that have greater kinetic energies will be deposited onto substrates above the MEC, and only particles that reach the evaporation without colliding are deposited below the MEC.

Diffraction patterns with concentric sets of rings, diffraction points or both were obtained in the electron diffraction studies for all systems studied. Ring diameter measurements allowed us to determine the interplanar distance. An Au standard was used to determine the K constant in order to perform calculations corresponding to interplanar distances (phases were assigned by comparison with reference data (JCPDS) [31] for SnO orthorombic and tetragonal, SnO_2 tetragonal β- and α-Sn. Table II summarizes the values obtained for some representative samples, as well as crystalline plains that justify the interplanar distances from the diffraction patterns shown in Fig. 4 (a-d).

It may be noted that the most crystalline phases correspond to metallic tin and tetragonal SnO.

Particles above the MEC presented the same tetragonal SnO (101), α-Sn (311) and (422) crystallographic phases, and it is probable that the formation of SnO produced by the oxygen absorbed on the metal surface (powder) that was used in the MVC reaction.

TABLE II. Crystalline spaces and assignments for Sn-Nps deposited on glass substrate.

Distance MEC (cm)	d(hkl) Determined	Crystalline phases and planes assigned		d(hkl) Experimental
(-)10	2.980	SnO(Tetragonal)	(101)	2.989
	2.290	α-Sn	(200)	2.294
	2.679	SnO(Tetragonal)	(110)	2.688
	2.287	α-Sn	(220)	2.294
(-)3	1.614	α-Sn	(400)	1.622
	1.486	α-Sn	(331)	1.489
	2.994	SnO (Tetragonal)	(101)	2.989
(+)3	1.940	α-Sn	(311)	1.956
	1.322	α-Sn	(422)	1.325
	2.991	α-Sn	(101)	2.989
(+)10	1.944	α-Sn	(311)	1.956
	1.331	α-Sn	(422)	1.325

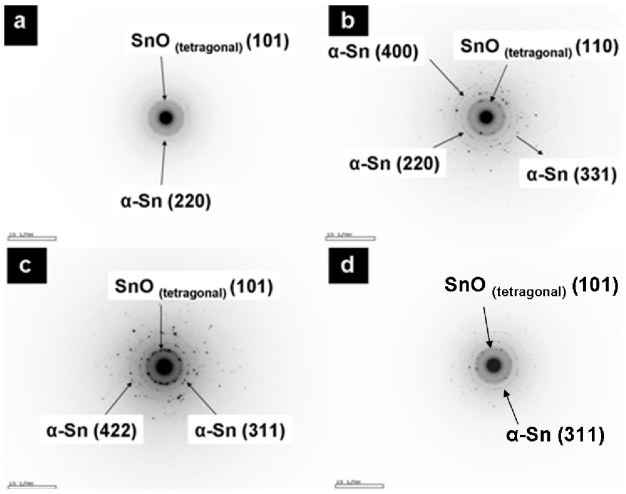

FIGURE 4. Diffraction patterns of deposits corresponding to the following distances from the MEC: (a) (-) 10 cm (b) (-) 3 cm, (c) (+) 3 cm and (d) (+) 10 cm

Synthesized nanoparticles were mainly polycrystalline and formed by very small crystallites oriented randomly, which provide few diffraction rings.

Tetragonal SnO has also been reported in studies including thermal treatment of films and Sn metallic particles [32,33]. For particles deposited below the MEC, (311) and (422) α-Sn phases were the preferential orientations. These orientations would explain the deposition mechanism and further nucleation on the substrate surface.

Figures 5a and 5b show the dark field TEM micrographs of the first and second ring observed with the electron diffraction pattern for Sn-Nps deposited at (+) 10 cm to the MEC,, where the white spots correspond to particles of α-Sn and SnO, respectively.

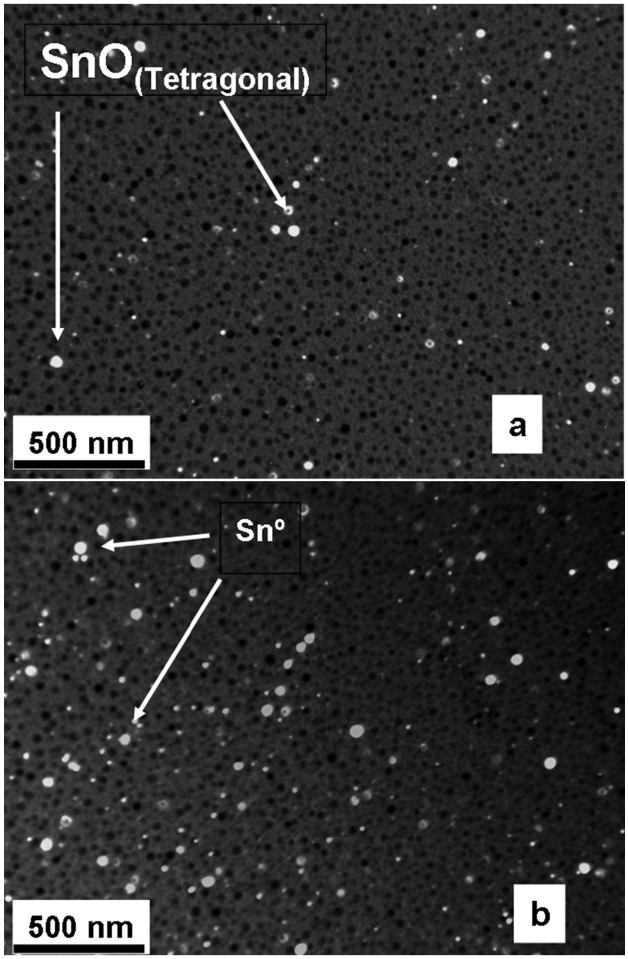

FIGURE 5. Dark field micrograph of (+) 10 cm to MEC, for MEM2 evaporated. (a) First ring, (b) second ring.

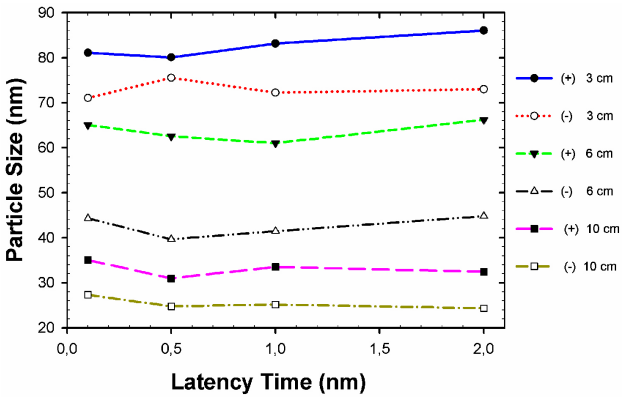

FIGURE 6. Variation in latency time according to the size of the deposited particles.

On the other hand, the effect of latency time after Sn-Nps depositions did not significantly affect the particle size. Figure 6 shows the trend in particle size according to time. This graph indicates that the particle size is not affected by variations in latency time. Quite the opposite occurs with the variation in latency time in CLD technique, producing a modification of structure and nanoparticle size [21].

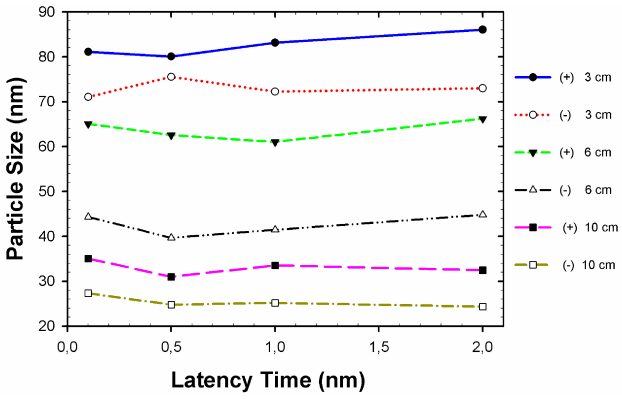

FIGURE 7. Metal evaporated moles (MEM) for (-) and (+) 6 cm, according to particle size.

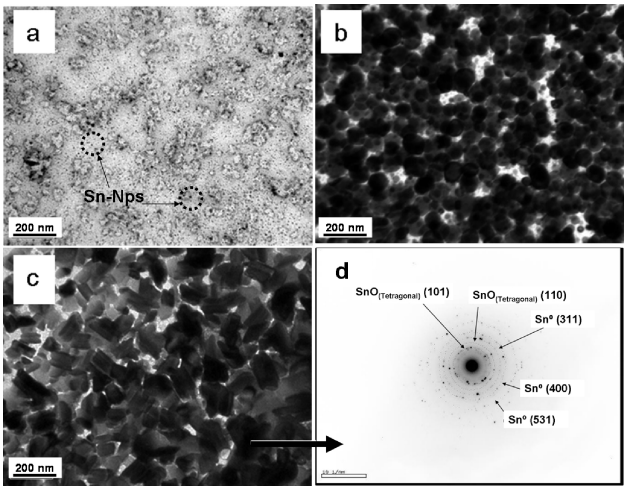

FIGURE 8. Metal evaporated moles (MEM) for (+) 6 cm depending on particle size. Micrographs for MEM1 (a), MEM2, (b-c) MEM3, (d) and electron diffraction of MEM2.

In CLD, the particles are trapped with solvent in a frozen matrix. When the defrosting of the matrix begins, particles collide and form clusters. This nucleation process is dominated by metal-solvent interactions and metal diffusion in the frozen matrix. Nucleation kinetics also depend on the defrosting speed of the matrix, producing smaller particles at greater latency times.

In MVC, particle size is not affected by variation in latency time because Nps are formed at the time that atoms are deposited on the substrate surface at 77 K. In the absence of solvent within a frozen matrix, such as in MVC reactions, the variation of latency time does not affect particle size because these particles lack mobility on the substrate.

The nucleation probabilities during the film formation of nanoparticles in the thermal evaporation system have been very controversial. The experimental evidence proposed by Barnes *et al.* [34] is only applicable to the charged cluster model grown by CVD.

Particle size is also affected by the MEM, due to the large number of atoms in the gaseous state that increase the collision probability.

TABLE III. %T of Sn-Np films at λ_{800}nm (-) 3, 6, and 10 cm to the MEC and (+) 3, 6 and to the MEC for MEM1

MEC (cm)	Substrate Position (-)Below, (+)Above	T (λ_{800} nm) %
3	(-)	22
	(+)	20
6	(-)	16
	(+)	11
10	(-)	8
	(+)	3

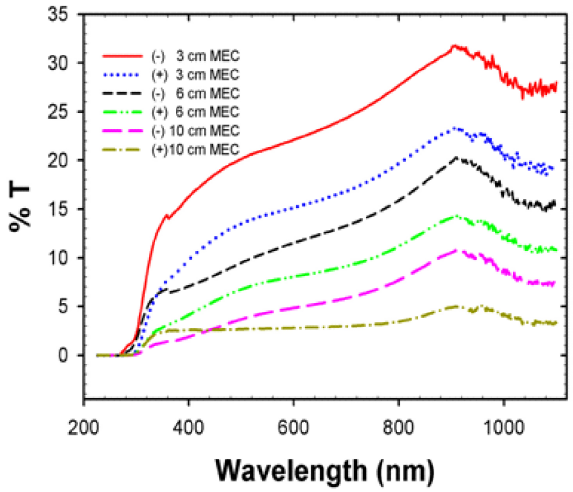

FIGURE 9. UV-Vis spectra of Sn-Np films on glass substrates for (-) 3, 6 and 10 cm to the MEC and (+) 3, 6 and 10 cm to the MEC for mem1.

Figure 7 shows the MEM for (-) and (+) 6 cm to the MEC, depending on particle size. Regular spherically shaped particles with an average size of 10 nm were obtained for MEM1, and irregularly shaped particles with an average size of 125 nm were produced for MEM3. For MEM3, crystalline phases corresponding to tetragonal SnO and α-Sn were observed, as well as for mem1 and mem2. See Fig. 8.

Sn-Nps on glass substrates were studied by UV-Vis spectroscopy; the corresponding spectra are shown in Fig. 9. Spectra were recorded for MMM1 at distances of (–) and (+) 3, 6 and 10 cm to the MEC.

Table III summarizes the transmittance percentage (%T) of the deposits. The deposits below the MEC presented lower %T than the deposits above the MEC. For mem1, at (-) 3 and (+3) cm, the %T at λ_{800} nm were 22 and 11, respectively. Mem1 shows a similar pattern of transmittance, with 16 and 12 at (-) and (+) 6 cm, respectively. The differences in transmittance values are due to the formation of multi-layer metallic films with different thicknesses before the creation of real nucleation sites. For (+), (-) 6 and (+), (-) 10 cm, deposits are less transparent because the layers formed are thicker. Figure 10 shows the TEM micrographs of multi-layer Sn-Np films.

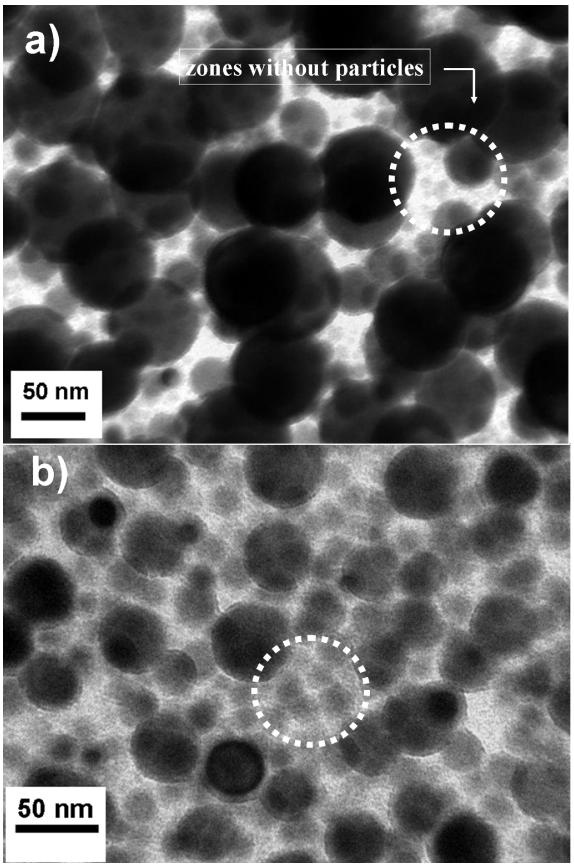

FIGURE 10. TEM micrographs of Sn-Np films (a) (-) 3 cm to the MEC, zones without particles can be observed. (b) (+) 10 cm to the MEC, shows layer formation.

4. Conclusions

Metallic vapor condensation is an effective technique to obtain different sizes of Sn-Nps. The distance between the substrates and the metal evaporated center is the main parameter affecting the particle size, producing regular spherical particles. Nanoparticle shape varies significantly with the metal evaporated moles. Deposited nanoparticles are formed by tetragonal SnO and α-Sn in all deposits obtained. Variation of latency time neither affected the size nor the shape of nanoparticles. UV-Vis analysis evidenced multi-layer film formation, with thickness depending on the distance to the MEC. MVC permits the synthesis of thin metallic films that can be oxidized in order to produce semiconductor films with electronic applications.

Acknowledgements

This research was supported by Fondecyt 1040456. The authors would also like to thank Serveis Cientificotècnics of the Universitat de Barcelona, Spain for the use of the ESEM and AFM equipment. SEM and TEM analyses were performed at the Electron Microscopy laboratory of the Universidad de Concepción, International Center for Nanotechnology and Advanced Materials University of Texas at San Antonio and the Laboratorio de Propiedades Opticas de Materiales of the Universidad Nacional de Colombia-Manizales.

1. K. Suenaga *et al*., *Science* **278** (1997) 653.
2. S. Sun, C. B. Murray, D. Weller, L. Folks, and A. Moser, *Science* **287** (2000) 1089.
3. W. S. Liao, T. Yang, E. T.Castellana, S. Kataoka, and P. S. Cremer, *Adv. Mater*. **18** 2240.
4. G. Schmid, *Chem. Rev*. **93** (1992) 1709.
5. L. N. Lewis, *Chem. Rev.* **92** (1993) 2693.
6. G. Cárdenas, Y. León, Y. Moreno, and O. Peña, *Colloid Polym Sci.* **284** (2006) 644.
7. F. Gu, S. F. Wang, M. K. Lü, G. J. Zhou, and D. Yuan, *J. Phys. Chem. B* **108** (2004) 8119.
8. Z. W. Chem, J. K. L. Lai, C. H. Shek, and H. D. Chen, *Appl. Phys A* **81** (2005) 959.
9. L. M. Cukrov, T. Tsuzuki, and P. G. McCormick, *Script Mater* **44** (2001) 1787.
10. J. J. Zhu, Z. H. Lu, S. T. Aruna, D. Aurbach, and A. Gedanken, *Chem. Mater* **12** (2000) 2557.
11. T. Nütz, and M. Haase, *J. Phys. Chem B* **104** (2000) 8430.
12. G. Cárdenas, *J. Chil. Chem. Soc.* **50** (2005) 603.
13. G. Cárdenas, R. Segura, and J. Reyes-Gasga, *Colloid Polym Sci*, **282** (2004) 206.
14. G. Cárdenas, K. J. Klabunde, and E. Dale, *Langmuir* **3** (1987) 986.
15. V. Lavayen *et al*., *Appl. Surf. Sci*, **253** (2007) 3444.
16. M. T. Reetz and W. J. Helbig, *Am. Chem. Soc.* **116** (1994) 7401.
17. T. Tano, K. Esumi, and K. Maguro, *J. Colloid. Interf. Sci* **133** (1989) 530.
18. W. X. Chem, J.Y. Lee, and Z. Liu, *Chem. Commun* (2002) 2588.
19. K. J. Klabunde, Y. X. Li, and B. J. Tan, *Chem. Mater* **3** (1991) 30.
20. Y. Koltypin, G. Katabi, G. Cao, R. Prozorov, and A. Gedanken, *J. Non-Cryst Solids* **159** (2001).
21. R. Segura and G. Cárdenas, *J. Crystal. Growth* **310** (2008) 495.
22. M. J. Yacamán and R. F. Mehl, *Metal Mater. Trans. A* **29** (1998) 713.
23. A. Henglein, *Chem. Rev.* **89** (1989) 1861.
24. T. Trindade, P. O'Brien, and N. L. Pickett, *Chem. Mater.* **13** (2001) 3843.

25. J. H. Fendler and F. C. Meldrum, *Adv. Mater*. **7** (1995) 607.

26. G. Cárdenas, S. Salinas and R. Oliva, *Colloid Polym. Sci.* **282** (2003) 41.

27. Li. Zhiwei *et al.*, *Ultrason. Sonochem* **14** (2007) 89.

28. Z. Yanbao, Z. Zhijun, and D. Hongxin, *Mat. Sci. Eng. A* **359** (2003) 405.

29. M. Han *et al.*, *Nucl. Instrum. Meth. B* **135** (1998) 564.

30. M. Kozlowski *et al.*, *Vacuum* **82** (2008) 956.

31. Powder Diffraction File, Inorganic Phases, JCPDS, International Centre for Diffraction Data, Pennsylvania, USA. 1997.

32. R. B. Patil, R. K. Puri, and P. Vijaya, *J. Alloy Compd*, **463** (2008) 453

33. E. P. Romashevskaya *et al*., *Thin Solid Films* **515** (2007) 6350.

34. M. Barnes *et al*., *J. Crystal Growth* **213** (2000) 83.